

Three-Body Photodissociation of 1,3,5-Triazine

T. Gejo, J. A. Harrison,[†] and J. Robert Huber*

Physikalisch-Chemisches Institut der Universität Zürich, Winterthurerstrasse 190, CH-8057 Zürich, Switzerland

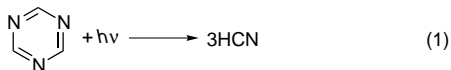
Received: April 2, 1996; In Final Form: May 28, 1996[⊗]

The three-body dissociation of 1,3,5-triazine ($\text{H}_3\text{C}_3\text{N}_3 \rightarrow 3\text{HCN}$) has been studied by molecular beam photofragment translational spectroscopy following excitation at 308, 295, 285, 275, 248, and 193 nm. The analysis of the measured translational energy distributions of the HCN photofragments has shown that the dissociation mechanism is not, as previously suggested, a symmetric (or synchronous) three-body process but rather is a two-step concerted process, where concerted refers to correlation between the asymptotic velocity vectors of the three ejected HCN fragments. Furthermore, there is evidence that the initially excited electronic state ($^1E''$, 1A_2) is deactivated by radiationless processes (internal conversion/intersystem crossing) to a lower electronic and finally dissociative state which is, according to symmetry correlation, the electronic ground state (electronic predissociation).

1. Introduction

The three-body dissociation process of a polyatomic molecule has attracted recent interest due to the mechanism which involves a simultaneous breaking of multiple bonds.^{1–19} Following absorption of a photon, a variety of molecules have shown a decay behavior which appears consistent with a synchronous or concerted three-body dissociation. Of particular interest in such studies is the energy disposal among the emerging fragments, as this information reveals features of the potential energy surfaces involved and the ensuing dynamics on these surfaces during dissociation. Among the molecules recently studied to gain insight in a three-body decay are acetyl iodide,² trifluoroacetyl iodide,⁴ 1,3,5-triazine,⁸ *s*-tetrazine,⁹ C_3O_2 ,¹⁰ acetone,^{13,14,17} CF_2I_2 ,^{15,16} and azomethane.^{18,19} In most cases these systems have been investigated at only a single photolysis wavelength, because of the difficult and lengthy nature of experiments that may involve up to three polyatomic fragments produced with varying amounts of internal excitation. One technique that has found widespread application is photofragment translational spectroscopy.^{20,21} This technique, though not fragment quantum state specific, provides sufficient versatility to allow examination of the recoil energy of all the fragments produced with reasonable resolution. Most of the molecules mentioned above have been studied by this method with 1,3,5-triazine (*s*-triazine or $\text{H}_3\text{C}_3\text{N}_3$) showing particularly intriguing features.

It is well established that *s*-triazine yields three HCN fragments following photolysis:⁸



The HCN dimer is not expected to have a significant binding energy,²² and it thus appears that it will not play an important role in the dissociation. Using photofragment translational spectroscopy Ondrey and Bersohn⁸ measured the translational energies of the HCN fragments produced at an excitation wavelength of 248 and 193 nm, which corresponds to a $n\pi^*$ type transition (from 230 to 320 nm) and to $\pi\pi^*$ and Rydberg transitions below 230 nm.²³ By arguing that the initial 3-fold

symmetry would be retained during the dissociation, they found that the HCN molecules each have an average kinetic energy of 10 kcal/mol at 248 nm but only 2 kcal/mol at 193 nm. Not only was the average translational energy much lower at the shorter wavelength but the translational energy distribution was also much narrower, indicating a considerable difference in the dissociation dynamics. Two different electronic dissociation channels cannot account for this feature since symmetry correlation shows that *s*-triazine must dissociate on the lowest potential energy surface in order to produce three ground state HCN molecules.⁸ At these wavelengths it is energetically impossible to populate the *A* electronic state of HCN. This intriguing result was rationalized as originating from a non-statistical distribution on the ground state due to rapid dissociation caused by the large amount of available energy. In an accompanying paper, Goates, Chu, and Flynn²⁴ reported that HCN produced from the 193 nm photolysis of *s*-triazine has a large amount of excitation in the bending mode. This finding appeared to be consistent with that of Ondrey and Bersohn because, on the basis of their idea, the difference of available energy is accounted for by the internal energy of HCN, more specifically, the increase of available energy allows the dissociation to proceed more rapidly since the HCN molecules do not have to relax as much from their initial bent geometry following photolysis at 193 nm compared to photolysis at 248 nm. The result of an *ab initio* calculation²⁵ also supports Ondrey and Bersohn's conclusion that all three HCN molecules possess equivalent translational energies as a consequence of the 3-fold symmetry of the predicted transition state.

As also observed,⁸ the comparative result between these two photolysis wavelengths appears to show a remarkable and unexpected behavior for the dissociation dynamics. If, indeed, a rapid dissociation causes a less statistical translational energy distribution in the HCN products, a decrease in the average translational energy at other, intermediate photolysis wavelengths should also be observed. The question of whether there is a gradual change in dynamics as the internal energy is increased or whether the change is due to a "memory" of the initial excited state which can be suddenly switched on upon accessing certain quantum states is, therefore, an open one at present. There is also some doubt about the symmetric three-body nature of the dissociation of *s*-triazine; apparently, the photon energy at 193 nm (148 kcal/mol) is not sufficient to break the three CN bonds simultaneously without a concomitant

[†] Permanent address: Department of Chemistry, Massey University, Albany, Private Bag 102-904, NSMC, Auckland, New Zealand.

[⊗] Abstract published in *Advance ACS Abstracts*, July 15, 1996.

change of geometry from the 120° HCN angle that exists in *s*-triazine.^{24,26,27} Due to the amount of relaxation of energy and geometry required before fragmentation can occur, one might reasonably expect that not all bonds will be broken simultaneously.

The present work deals with a reinvestigation of the photodissociation of *s*-triazine by photofragment translational spectroscopy at a variety of photolysis wavelengths. The use of an excimer laser and a dye laser pumped by a Nd:YAG laser has allowed us to measure the photofragment translational energy distributions over photolysis wavelengths ranging from 193–308 nm, which corresponds to a range in available fragment energy of between 105 and 53 kcal/mol. From the high-resolution TOF spectra obtained with our apparatus the dissociation of *s*-triazine is clearly shown to occur via a nonsymmetric route. On the basis of these results, we have simulated successfully this three-body dissociation by consideration of the expected angular distribution of photofragment recoil vectors. The simulations also provide information on the translational energy distributions due to primary and secondary dissociation.

2. Experimental Section

The experiments were carried out with the high-resolution PTS apparatus described previously.²⁸ A gas mixture was prepared by flowing helium carrier at a stagnation pressure of 500 mbar over a solid sample of *s*-triazine cooled to 20°C . A pulsed molecular beam of the gas mixture was generated either by means of a piezoelectrically driven pulsed valve or by a similar source with an additional heating element.²⁹ To avoid dimers, the photolysis laser pulse was timed to coincide with the leading edge of the beam pulse where monomer species dominate. The velocity distribution of *s*-triazine was measured by the hole-burning technique,³⁰ and was found to have a most probable velocity of 1000 and 1230 m/s and a beam translational temperature of 20 and 3 K with and without the heating element, respectively.

Time-of-flight (TOF) distributions of the photofragments were measured at several scattering angles Θ , where Θ is the angle between the molecular beam and the laboratory-fixed direction of the detection axis. The 193, 248, and 308 nm laser pulses were generated by an ArF, KrF, or XeCl excimer laser (Lambda Physik EMG 101 MSC), respectively. The 275, 285, and 295 nm laser pulses were obtained by frequency-doubling the output of a pulsed dye laser (Lambda Physik, SCANMATE 2E), which was pumped by the frequency-doubled output of a Nd:YAG laser (Continuum, Powerlite 7020). Typical laser fluences were 400 mJ/cm^2 at 193 nm, 500 mJ/cm^2 at 248 nm, 80 mJ/cm^2 at 275, 285, and 295 nm, and 2.0 J/cm^2 at 308 nm. After a flight path of 34.5 cm the photofragments were ionized by electron bombardment, discriminated according to their mass-to-charge ratio (m/e) within a quadrupole mass filter, and detected by an electron multiplier. A time offset of $3.9(m/e)^{1/2}$ ms was subtracted from all of the TOF spectra before analysis in order to correct for the ion flight time through the quadrupole mass spectrometer.

To measure the recoil anisotropy of the photofragment flux, a 248 nm laser beam was polarized to a degree of $91 \pm 1\%$ using a stack of 10 quartz plates placed at Brewster's angle to the laser beam. Polarized TOF spectra were taken at four polarization angles ϵ , where the latter defines the angle between the electric vector of the polarized laser beam and the detection axis. The polarization angle was rotated by means of a half-wave plate placed after the quartz plates stack.

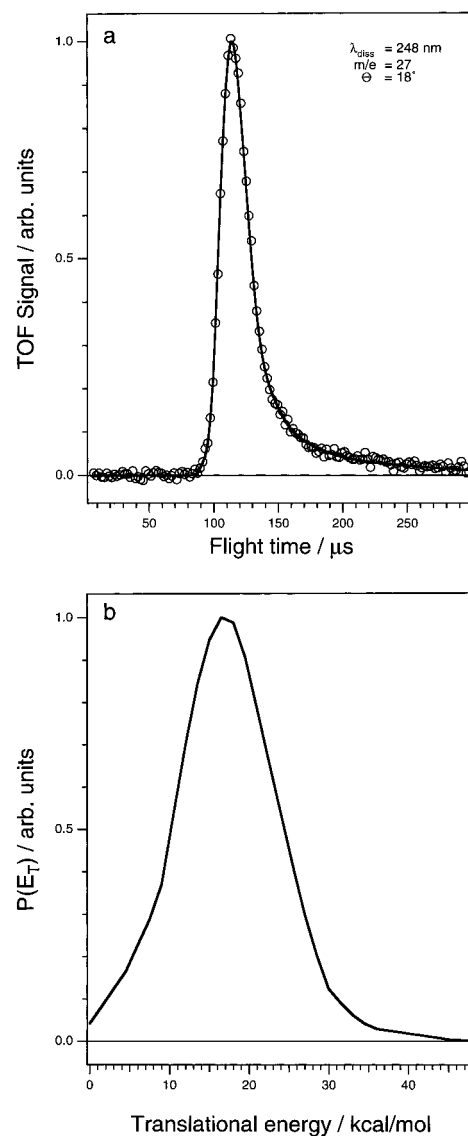


Figure 1. (a) TOF distribution of HCN fragment from photodissociation of *s*-triazine at 248 nm. The circles represent the experimental data, the solid line is the best fit obtained from the translational energy distribution shown in (b). (b) Center-of-mass translational energy distribution $P(E_T)$ of the HCN fragment.

3. Results

3.1. Excitation at 248 nm. Photofragment signals were observed with the mass filter set at $m/e = 27$ (HCN^+) while no signal was detected for the mass to charge ratio, $m/e = 54$ ($\text{H}_2\text{C}_2\text{N}_2^+$). The unpolarized TOF spectra for $m/e = 27$ at $\Theta = 18^\circ$ are displayed in Figure 1a. The solid line corresponds to the calculated best fit distribution, which was obtained by a forward convolution procedure³¹ of the center-of-mass (CM) translational energy distribution $P(E_T)$ for the HCN fragment, shown in Figure 1(b). This $P(E_T)$ refers to the translational energy of each HCN molecule as measured directly from the time-of-flight spectrum. The overall $P(E_T)$ for the dissociation process also includes the kinetic energy of the partner fragment(s).^{21,31} Owing to the complex nature of the dissociation that may include three fragments, it is not possible to unambiguously decide a priori what the overall $P(E_T)$ will be, as this will depend upon the recoil velocity vector distribution for the other fragments. This point and the model eventually used to fit the distribution are addressed in the Discussion section. It should be noted that although the total $P(E_T)$ distribution does depend upon the particular model used, the average $P(E_T)$ must

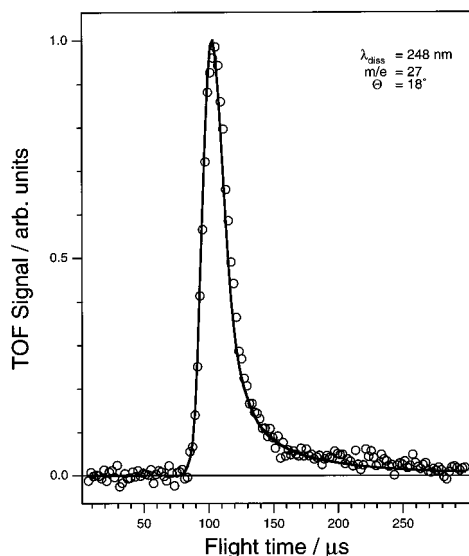


Figure 2. TOF distribution of HCN fragments from photodissociation of *s*-triazine at 248 nm. As in Figure 1a but with the molecular beam generated by the heated source.

be the same for any model and will correspond to the average value observed in the TOF spectra.

Figure 1a shows the TOF signal which gradually decreases around 200 μs . To confirm that the effect of clusters in this region can be ignored, photofragment signals were measured and the $P(E_T)$ distribution was determined through the use of the heated nozzle ($T \sim 200^\circ\text{C}$) pulsed beam source.²⁹ The result is depicted in Figure 2. Although there is an apparent difference between the two distributions shown in Figures 1a and 2, these differences can be entirely attributed to slight differences in the beam conditions. Once these are accounted for, the two time-of-flight spectra can be fitted using the same $P(E_T)$, which proves the contribution from cluster photolysis to the $m/e = 27$ signal to be negligible.

The threshold (or upper limit) of the translational energy for the fastest fragments was determined to be 48 kcal/mol as indicated by the $P(E_T)$ of Figure 1b. To ensure that multiphoton absorption does not affect the threshold, TOF distributions were measured with laser fluences ranging between 270 and 1100 mJ/cm^2 at $\Theta = 45^\circ$. The result is shown in Figure 3. Though there is clearly an increase in signal corresponding to the fastest HCN molecules at the highest laser fluence used, the shapes of the photofragment signals remained constant below a laser fluence of 560 mJ/cm^2 . We conclude that two-photon processes are not important below a fluence of 500 mJ/cm^2 and hence that the one-photon process has a threshold translational energy of ~ 48 kcal/mol.

Figure 4 shows the polarized TOF spectra for $m/e = 27$ taken at $\Theta = 18^\circ$ with $\epsilon = -20^\circ$ and 70° . Four independent measurements ($\epsilon = -20^\circ, 70^\circ, -70^\circ,$ and 20°) were carried out, but no significant polarization effect was observed. Thus, the fragment anisotropy parameter β ³² must have a value close to zero. Because the peak should consist of three types of HCN fragment (corresponding to the three recoil velocity vectors), it is not possible to determine a small β value precisely. Nevertheless, in view of the observation of *s*-triazine fluorescence around 310 nm,³³ the measured value of $\beta \approx 0$ is presumably due to a relatively long lifetime of the initially excited state of *s*-triazine.

The available energy is given as $E_{\text{avl}} = h\nu - D_0 + E_{\text{int}}$, where $h\nu$ is the photon energy, D_0 is the bond dissociation energy, and E_{int} is the internal energy of the parent molecule.²¹ The latter can be neglected for supersonic jet expansion. On the

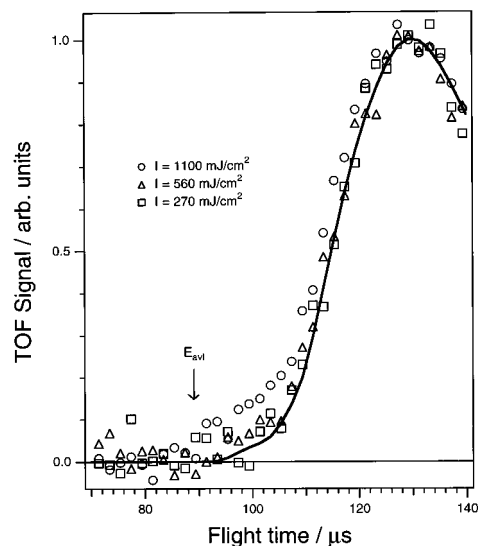


Figure 3. TOF distributions of the HCN fragments from 248 nm photodissociation of *s*-triazine using three different laser fluences as indicated. The solid line is the forward convolution of $P(E_T)$ given in Figure 1b.

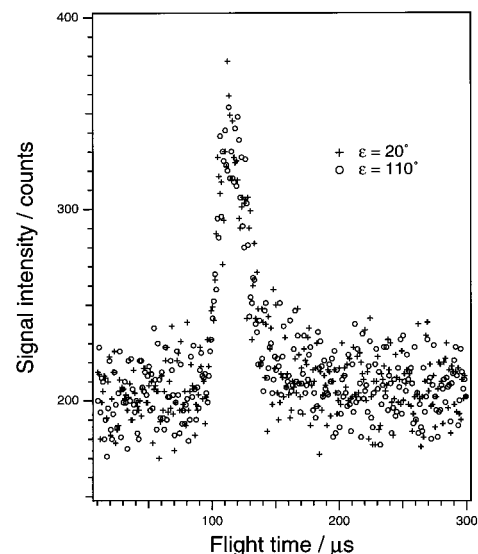


Figure 4. Polarized TOF distribution of HCN fragments of *s*-triazine at 248 nm and $\Theta = 45^\circ$. The two set of data were taken with polarization angles of $\epsilon = -20^\circ$ and $+70^\circ$.

basis of the formation enthalpies of *s*-triazine and HCN, the cleavage of all three bonds requires a dissociation energy $D_0 = 39.6$ kcal/mol.^{24,26,27} Consequently, the available energy is 75.7 kcal/mol following excitation at 248 nm (115.3 kcal/mol). The $P(E_T)$ distribution of the detected HCN fragments at 248 nm (Figure 1b) shows an average value of 17.4 kcal/mol, which results in an average total translational energy release of 52.2 kcal/mol. This would correspond to 69% of the available energy and implies that the three HCN fragments are formed with a remarkably high translational energy and with only 7.8 kcal/mol of internal energy in each HCN molecule. The observed $P(E_T)$ with the threshold translational energy of 48 kcal/mol per HCN molecule is unequivocal evidence that the 3-fold symmetry during dissociation is not preserved for a substantial number of the dissociating molecules because their sum would simply exceed the available energy (at least all those with $E_T > 25$ kcal/mol, see Figure 1b).

Finally, it is important to note that the TOF spectrum was also recorded under scattering angles $\theta = 12^\circ, 30^\circ,$ and 60° . In all cases only a single peak was obtained. In comparison with

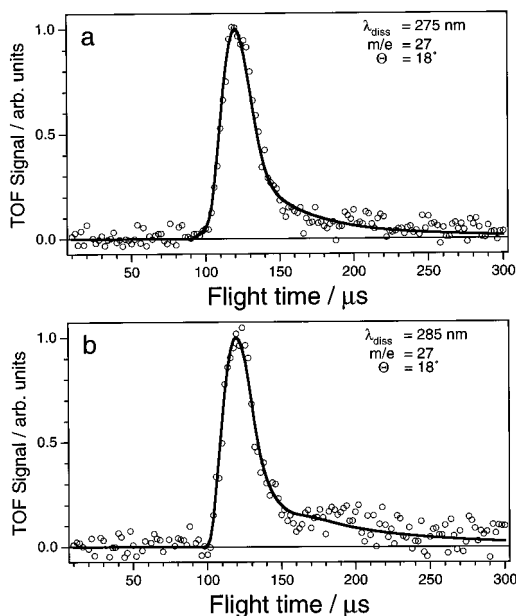


Figure 5. TOF distribution of HCN fragments from photolysis of *s*-triazine at (a) 275 and (b) 285 nm. The circles represent the experimental data. The solid lines are obtained from the $P(E_T)$ distributions shown in Figure 6.

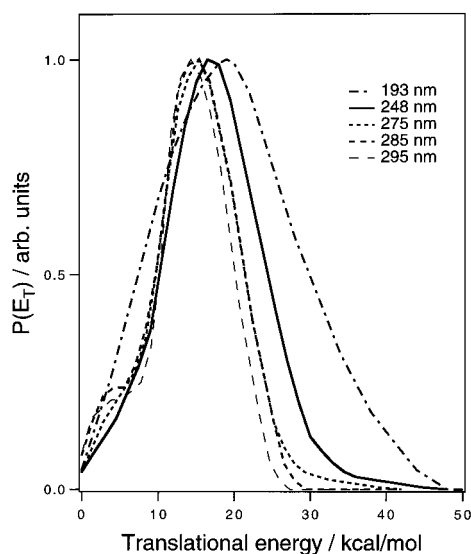


Figure 6. Best-fitting translational energy distributions $P(E_T)$ of HCN from photolysis at 193, 248, 275, 285, and 295 nm. $P(E_T)$ is shown as a function of HCN translational energy in the center-of-mass system of *s*-triazine and hence does not include any contribution from the partner fragments.

the spectrum in Figure 1a, the peak was slightly broader at 60° and slightly narrower at 12°.

3.2. Excitation at 275, 285, and 295 nm. We measured the photofragment TOF spectra with mass setting at $m/e = 27$ (HCN^+) and $\Theta = 18^\circ$ for the photolysis at 275, 285, and 295 nm. Figure 5, a and b, displays the spectra taken at 275 and 285 nm, respectively. The solid lines represent the best fit from the forward convolution with the $P(E_T)$ distributions shown in Figure 6. It should be noted that the laser light was polarized with $\epsilon = 0^\circ$ although the measured anisotropy $\beta \cong 0$ at 248 nm suggests that this will not affect the TOF spectra. The much weaker laser power at these excitation wavelengths accounts for the lower signal-to-noise ratio as compared to the 248 nm photolysis TOF spectrum. The shape of the $P(E_T)$ is not significantly different from that obtained at 248 nm (Figure 1b), though the position is slightly changed due to the change in

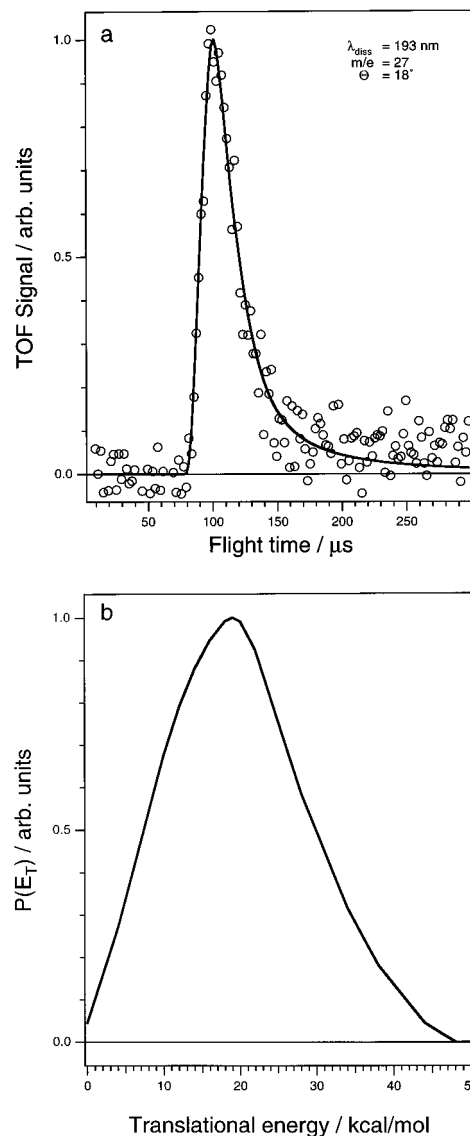


Figure 7. (a) TOF distribution of HCN fragments from photolysis at 193 nm. The circles represent the experimental data, and the solid line is the best fit obtained from $P(E_T)$ shown in Figure 6. (b) $P(E_T)$ distribution calculated from the TOF spectrum at 193 nm.

available energy. The average translational energy $\langle E_T \rangle$ obtained from the $P(E_T)$ distributions given in Figure 6 is 15.2 kcal/mol at 275 nm, 14.7 kcal/mol at 285 nm, and 13.8 kcal/mol at 295 nm. These average translational energies correspond to about 70% of E_{avl} (Table 1).

3.3. Excitation at 193 nm. Figure 7a shows the photofragment signal at $m/e = 27$ from photolysis at 193 nm (148 kcal/mol) using the heated source. Only a very weak signal was observed when using the source without the heating element. The room temperature absorption spectrum of *s*-triazine shows a broad absorption band with an absorption coefficient of ~ 100 L/(mol·cm) at 193 nm. The strongly reduced signal for the unheated source is probably due to a small absorption coefficient at 193 nm for jet-cooled *s*-triazine. The $P(E_T)$ distribution calculated from the TOF spectrum at 193 nm is displayed in Figure 7b and reveals an average translational energy of the HCN fragments of 19.8 kcal/mol. Despite the fact that there is only a small difference of 2.4 kcal/mol in the average translational energy of the HCN photofragments between photolysis at 193 and 248 nm, the shape of the distribution is noticeably wider at 193 nm while the threshold of translational energy remains at ~ 48 kcal/mol. The average

translational energy of $3 \cdot 19.8$ kcal/mol corresponds to $\sim 55\%$ of E_{avl} .

Using the heated source, we expected to obtain a better Franck–Condon overlap for absorption without affecting the dynamics. In the present case symmetry correlation indicates that *s*-triazine dissociates on the lowest potential energy surface.⁸ This dissociation therefore includes electronic relaxation as a necessary step, which suggests that absorption involving different Franck–Condon factors should not significantly influence the dynamics (*vide infra*).

3.4. Excitation at 308 nm. Figure 8 shows the photofragment signal for $m/e = 27$ detected at $\Theta = 45^\circ$. In view of the similarity to the $P(E_T)$ measured at 193 nm, the photofragments were produced not only by a one-photon but also by a two-photon process. The threshold translational energy of ~ 50 kcal/mol also supports involvement of a two-photon process, because the high translational energy exceeds the limits imposed by conservation of momentum for a one-photon process. Although the energy dependence was measured over the range from 1000 to 2000 mJ/cm², the integrated TOF signal is not proportional to the square of the laser power, indicating that the TOF spectrum contains more than two components. To clarify this point, we examined the possibility of fitting the TOF signal with three energy distributions, two of which are the same as the $P(E_T)$ distributions obtained at 295 and 193 nm and the third one being a low translational energy $P(E_T)$. The solid line through the data points in Figure 8 is the result of the fit using these three distributions. The first two $P(E_T)$ distributions correspond to one- and two-photon excitations while the third $P(E_T)$, which is used to fit the low-energy region of the TOF spectrum, is presumably due to the contribution of cluster photolysis considering the low signal intensity. Such a situation would arise if the UV absorption is shifted to longer wavelength upon cluster formation, even though the photolysis laser pulse was timed to coincide with the leading edge of the beam pulse.

4. Discussion

4.1. General Aspect. There are two likely mechanisms for the photodissociation of *s*-triazine. The first one involves a symmetric single step (eq 1) while the second one proceeds according to a sequential process



In the case of reaction 1 the three HCN fragments will have identical kinetic energies in the center-of-mass frame of the *s*-triazine molecule, and thus we refer to this pathway as the symmetric three-body (synchronous) dissociation channel (Figure 9). The TOF spectrum will consist of a single peak, and the high-energy threshold of the HCN translational energy distribution will be at most equal to one-third of the available energy. The measured TOF spectra and the corresponding $P(E_T)$ (see Figures 1 and 7) show clear evidence that a substantial number of the fragments are ejected with E_T exceeding this threshold. Therefore, reaction 1 cannot be the dominant dissociation pathway that is operative following excitation between 193 and 248 nm. We are forced to consider reaction 2 with the intermediate $\text{H}_2\text{C}_2\text{N}_2$ which undergoes a secondary dissociation to form 2 HCN molecules. The second step 2b may occur on a similar time scale as the initial fragmentation step 2a or on a much longer time scale.

If the processes 2a and 2b occur on similar time scales, the dissociation may be considered to be a concerted process as

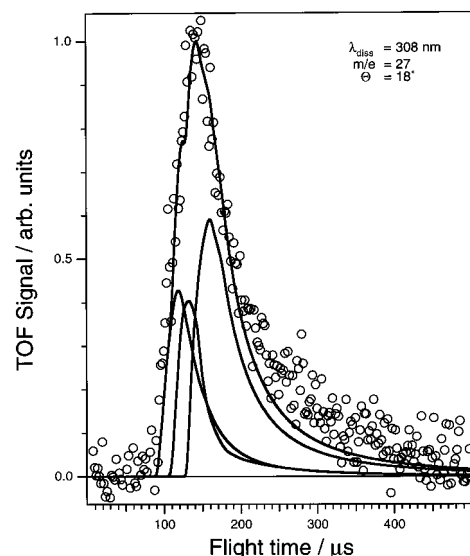


Figure 8. TOF distribution of HCN fragments from photolysis at 308 nm. The over all solid line is the fit consisting of three translational energy distributions (see text).

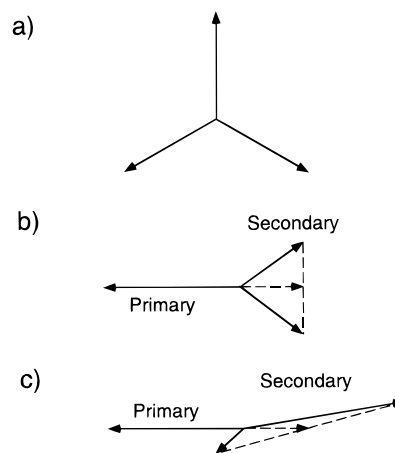


Figure 9. Vector diagrams for the three cases of photodissociation processes considered in this work. (a) a simultaneous symmetric three-body dissociation, with all three fragments having identical kinetic energies; (b) three-body dissociation in which the two HCN fragments generated in the secondary dissociation are ejected at the same angle to the initial primary dissociation recoil vector; (c) concerted (but asymmetric) three-body dissociation with one fragment ejected forward with respect to the recoil direction of the primary $\text{H}_2\text{C}_2\text{N}_2$ fragment.

long as the intermediate lifetime is shorter than a rotational period (*vide infra*). In the limiting case the $\text{H}_2\text{C}_2\text{N}_2$ moiety will not have had time to rotate, so that the two HCN fragments from step 2b will be ejected with the same speed. Since in this scenario the initial symmetry is essentially preserved, the decay is referred to as a symmetric sequential dissociation shown schematically in Figure 9. The symmetric three-body dissociation is obviously a limiting case of this latter process. If, however, the lifetime of $\text{H}_2\text{C}_2\text{N}_2$ is sufficiently long so that this fragment can undergo rotation, the velocity vectors of the two HCN fragment will generally have different magnitudes; this process corresponds to an asymmetric, sequential dissociation.

4.2. Modeling. We started the modeling of the observed time-of-flight spectra by considering the existence of a long-lived $\text{H}_2\text{C}_2\text{N}_2$ intermediate surviving for several rotational periods before breaking apart and thus giving rise to a sequential or stepwise mechanism. To this end we have carried out TOF simulations based on a forward convolution procedure of the primary and secondary photofragments.^{3,34–36} For the sequential

dissociation processes the angular HCN distribution is symmetric with respect to forward–backward scattering about the center-of-mass frame of the *s*-triazine parent with the fragment flux peaking at an angle to the primary recoil direction.^{34,37,38} The maximum HCN translational energy threshold corresponding to all of the available energy being released in the primary fragmentation step would result in two-thirds of E_{avl} , which is ~ 50 kcal/mol for the photolysis at 248 nm. The very low signal observed around this energy (Figure 1b) originates from fragments consistent with this extreme limiting case and clearly indicates that most dissociation events occur with a smaller translational energy and hence with a significant amount of internal excitation in the HCN fragments and probably also in the $\text{H}_2\text{C}_2\text{N}_2$ fragment. However, the TOF spectrum based on a long-lived intermediate should exhibit a bimodal TOF distribution; the first peak due to the primary dissociation and the second, slower peak to the two HCN fragments formed in the secondary dissociation step. In view of the small binding energy of the HCN dimer of a few kcal/mol,²² the intermediate $\text{H}_2\text{C}_2\text{N}_2$ may have an internal energy of a few kcal/mol at most, if it is to live for a significant length of time. The low binding energy (the shallow potential energy) limits the amount of energy that may appear as translation in the secondary fragments. Our simulations showed for all cases involving a long-lived $\text{H}_2\text{C}_2\text{N}_2$ intermediate with reasonable HCN–HCN binding energies, two pronounced peaks in the modeled spectra. Thus, the single peak observed in the experimental HCN TOF spectrum rules out such a mechanism and indicates that a more concerted dissociation is operative.

Having ruled out the symmetric three-body dissociation and the sequential or stepwise decay with a long-lived intermediate as dominant pathways, we attempted to model the single observed TOF peak by allowing (i) the two HCN fragments from dissociation of $\text{H}_2\text{C}_2\text{N}_2$ to have a significant amount of translational energy and (ii) the $\text{H}_2\text{C}_2\text{N}_2$ intermediate to have a finite lifetime for *partial* rotation. In general, when treating the sequence of an ABC-type reaction,^{34–36} one analyzes the TOF distribution of C in order to determine the recoil distribution of the primary photofragment pair AB and C. With this information, one simulates the TOF distributions of the secondary fragments A and B with the final recoil velocity vectors. In the case of *s*-triazine, however, the dissociation yields three indistinguishable HCN fragments which contribute to the TOF spectrum. Therefore, we simulated a sequential dissociation mechanism in the following manner. As a first step, the $P(E_T)$ of the primary dissociation was determined from the central region of the TOF spectrum (for example the region of 100–140 μs in Figure 11a). Secondly, the whole TOF spectrum was subsequently calculated using a variety of assumed $P(E_T)$ and angular distributions for the secondary dissociation step (see Figure 10). The secondary $P(E_T)$ and the angular distribution were varied until an acceptable fit had been obtained.

The analysis of a concerted three-body dissociation developed by Zhao et al. for *s*-tetrazine⁹ used a Gaussian function to express the spread about the asymptotic velocity vectors of secondary photofragments. We explored fitting the data with this function, but the result was unsatisfactory; the distribution required a function more strongly peaked at 90° to the primary recoil vector. Therefore, fitting was attempted by a Lorentzian angular distribution function shown in Figure 10a. The scattering angle δ is the angle between the recoil vector of the secondary dissociation and the direction of the primary dissociation. Since the final angular distribution should also include the process with the strong back and forward peak resulting from symmetry reasons^{34,37,38} as explained for the long-

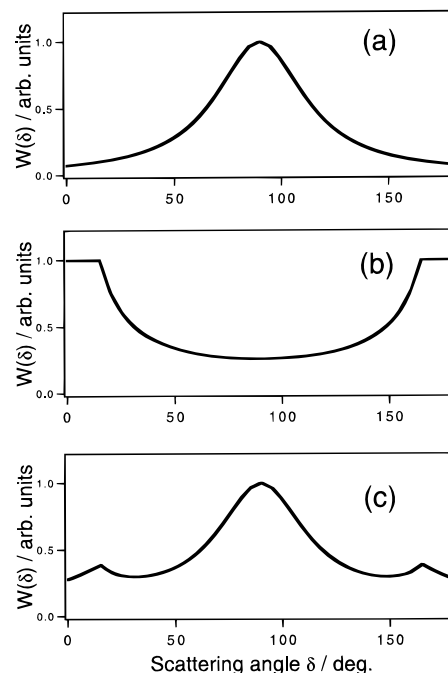


Figure 10. Angular distribution of the secondary photofragments. (a) angular distribution based on a Lorentzian at a center of 90° ; (b) $W(\delta)$ according to eq 3; (c) angular distribution obtained by superimposing (a) and (b).

lived case above, we satisfied this requirement by using the expression

$$W(\delta) = c \sin \delta^* / \sin \delta \quad (3)$$

for $\delta \in [\delta^*, 180^\circ - \delta^*]$ and $W(\delta) = c$ otherwise. This distribution is shown in Figure 10b for $\delta^* = 20^\circ$. The final angular probability distribution shown in Figure 10c arises from a superposition of these two functions depicted in Figures 10a,b. A reasonable fit for the data at 248 nm was obtained using the $P(E_T)$ distributions for the primary and secondary dissociation shown in Figure 11b and the angular distribution with a center of 90° shown in Figure 10c.

Figure 11a depicts the TOF distribution of the HCN fragments from the 248 nm photodissociation and the partitioning into the two components. The component of the primary HCN fragments corresponds to the narrower peak and the broader peak to the HCN molecules from the secondary dissociation. The primary and secondary $P(E_T)$ distributions have similar mean values and comparable widths (Figure 11b). As is evident from Figure 11a, the fastest fragments arise from the dissociation of the $\text{H}_2\text{C}_2\text{N}_2$ due to scattering from secondary dissociation in the opposite direction relative to the velocity vector of the primary HCN fragment. On the other hand, the slowest fragments are those ejected from the secondary dissociation along the direction of the velocity vector of the primary HCN. A dissociation geometry corresponding to a case close to this situation is drawn in Figure 9.

On the basis of this analysis an interpretation of the decay mechanism rests on a sequential breaking of bonds. Since *s*-triazine is a cyclic compound, three bonds are eventually broken. Initially two bond fissions are required to release the primary HCN fragment, and subsequently a third fission is necessary during the secondary dissociation of the $\text{H}_2\text{C}_2\text{N}_2$ fragment. The latter decay involves a range of secondary dissociation recoil vectors with a scattering angle distribution strongly peaked at $\delta = 90^\circ$ indicating that the majority of fragmentations proceed with a small amount of rotation,

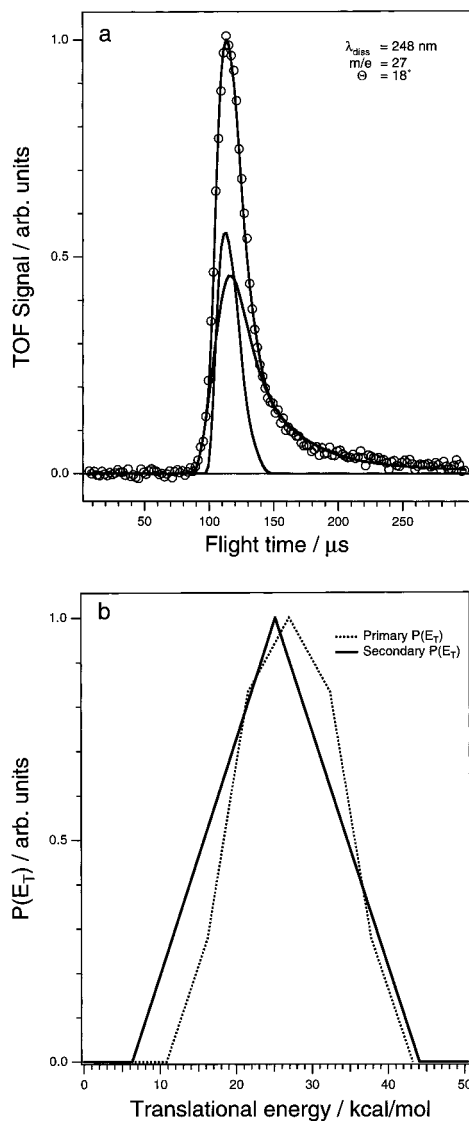


Figure 11. (a) TOF distribution of HCN fragments from photolysis at 248 nm. The circles represent the experimental data, and the solid lines are calculated TOF distributions obtained from the $P(E_T)$ s in (b) assuming a concerted process with $W(\delta)$ shown in Figure 10c. (b) Primary and secondary distributions, $P(E_T^1)$ and $P(E_T^2)$, of HCN.

noticeably less than a full rotational period, of the $\text{H}_2\text{C}_2\text{N}_2$ intermediate. According to the definition given by Strauss and Houston,¹⁰ we may still regard the *s*-triazine photodissociation as concerted because it was found necessary to break all three bonds on similar time scales, i.e., less than a rotational period of the intermediate. Only under these conditions will a single TOF peak be observed.

The simulations for the photolysis at 193, 275, and 285 nm are displayed in Figure 12. In each case the $P(E_T)$ curves found for the primary and the secondary dissociation are similar in form to those at 248 nm, and also the angular distribution for the photofragments was comparable to that obtained from the fit of the 248 nm data.

4.3. Energy of the Photofragments. The average translational energy $\langle E_T \rangle$ is defined in terms of the center-of-mass system of the *s*-triazine parent molecule and is equal to the sum of the average translational energies released in the primary and secondary dissociation step, $\langle E_T^1 \rangle + \langle E_T^2 \rangle$. The TOF measurements of the HCN fragment yielded the translational energy distributions $P(E_T)$ collected in Figure 6 and the $\langle E_T \rangle$ values listed in Table 1 where we also included $\langle E_T^1 \rangle$ and $\langle E_T^2 \rangle$ obtained from partitioning of $P(E_T)$ into $P(E_T^1)$ and $P(E_T^2)$ from the

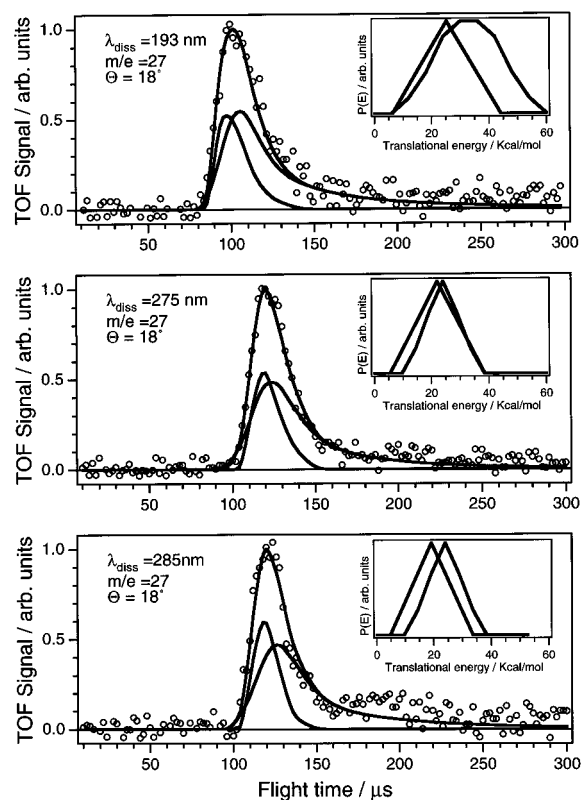


Figure 12. TOF distributions of the HCN fragments from photolysis at 193, 275, and 285 nm. The solid lines are calculated TOF distributions obtained from $P(E_T^1)$ and $P(E_T^2)$ shown in the insets for a concerted process.

TABLE 1: Partitioning of the Available Energy (E_{avl}) into the Translational (E_T) and Internal (E_{int}) Energy of the HCN Fragments upon *s*-Triazine Photolysis at Various Excitation Wavelengths^a

λ (nm)	E_{avl}	$\langle E_T \rangle$	$\langle E_{\text{int}} \rangle$	$\langle E_T \rangle / E_{\text{avl}}$ (%)	$\langle E_T^1 \rangle^b$	$\langle E_T^2 \rangle^b$
193	109	59	50	55	33	26
248	76	52	24	69	27	25
275	64	46	18	71	24	22
285	60	44	16	73	24	20
295	57	41	16	72		

^a All energies are in kcal/mol units. ^b From $P(E_T)$ partitioning.

primary and secondary dissociation shown in Figures 11 and 12. After photon excitation between 295 and 248 nm $\langle E_T \rangle$, which coincides approximately with the maximum of the $P(E_T)$ curve in Figure 6, is gradually shifted to slightly higher values and accompanied by a small broadening of $P(E_T)$. In all cases $\langle E_T \rangle$ represents about 70% of E_{avl} . A more pronounced change is evident if excitation occurs at 193 nm where $\langle E_T \rangle$ has decreased to ~55% of E_{avl} and $P(E_T)$ is considerably broadened compared to $P(E_T)$ at 248 nm. The behavior of the $P(E_T)$ distributions in Figure 6 is an indication that both dissociation steps are preceded by substantial intramolecular vibrational redistribution (IVR). As has been pointed out by Lee and co-workers,^{39–42} the translational energy release is, under these conditions, mainly correlated with the exit barrier along the reaction coordinate and is less influenced by the excess energy, and hence the excitation energy, when an appreciable exit barrier is involved. The $P(E_T)$ curves for different excitation energies (but for the same transition state) will therefore merely show a broader distribution at higher energy and a peak position change much smaller than the increase in the excess energy. This parallels our present observation. In recent three-body dissociation studies of azomethane,^{18,19} $\text{CH}_3\text{-N=N-CH}_3 \rightarrow \text{CH}_3 + \text{N}_2 + \text{CH}_3$, and acetone,¹⁴ $\text{CH}_3\text{-CO-CH}_3 \rightarrow \text{CH}_3 + \text{CO} +$

CH₃, similar $P(E_T)$ features were observed. Thus, the $P(E_T)$ distribution of azomethane photofragments measured at 193 nm¹⁹ was found to be similar to that at 351 nm, reported previously,¹⁸ and acetone excited at 193 and 248 nm produced similar photofragment distributions at the two excitation energies.¹⁴

The energy channeled into the internal degrees of freedom of the HCN fragment (see Table 1) is only ~30% of E_{avl} , except for 193 nm where it is ~45%. Under the latter conditions a substantial amount of E_{avl} is deposited into vibrational motion (much less into rotation), as observed by Goates et al.²⁴ who performed IR emission measurements on the HCN photoproducts. Moreover, they found that the number of quanta in the bending mode was very much greater than those in the CH stretching mode, indicating that the time for complete IVR relaxation to a statistical distribution is not sufficient in the dissociation process at 193 nm.

4.4. Mechanism. The absorption band of *s*-triazine in the excitation range 308–248 nm consists of two transitions:^{23,43} $^1A_1 \rightarrow ^1E''(n\pi^*)$ and $^1A_1 \rightarrow ^1A_2(\pi\pi^*)$. The excited state $^1E''$ is Jahn–Teller distorted and mixed via pseudo-Jahn–Teller interaction with the higher lying 1A_1 state.⁴³ The absorption band is highly structured, and below 300 nm fluorescence is observed.³³ It appears, therefore, that these two states are not directly dissociative; rather, they are deactivated by internal conversion and/or intersystem crossing³³ to a lower electronic state. Dissociation on the S_0 potential energy surface would then be consistent with the behavior of the fragment distributions $P(E_T)$ discussed above, where prior to dissociation substantial IVR occurs. Although excitation at 193 nm involves a different excited singlet state, it still leads to a fragment distribution the features of which are similar to those of the $P(E_T)$ distributions of the lower excitation energies. It is therefore conceivable that dissociation following 193 nm excitation occurs on the same potential energy surface as that using $\lambda \geq 248$ nm.

Since the *s*-triazine dissociation is clearly not a symmetric three-body process but a sequential one, the possible concertedness of the reaction is now considered within the definition appropriate to photofragment distribution measurements. Thus, using the rotational period of the intermediate species as a gauge, we consider a process uncorrelated or not concerted if the lifetime of the intermediate exceeds a rotational period.¹⁰ Under these conditions rotational averaging causes a complete loss of spatial correlation among the asymptotic velocity vectors of the primary and secondary photofragments.¹⁴ For *s*-triazine the analysis of the fragment distribution was shown to be successful only if the angular fragment distribution was assumed to be narrow, which clearly excludes rotational averaging. Consequently the three fragment velocity vectors are correlated, and the process can be considered to be concerted. More specifically, it is a two-step but still a concerted photodissociation, and there is evidence based on a highly structured absorption band, an isotropic fragment distribution ($\beta = 0$), and an only small $P(E_T)$ dependence on the excitation energy that dissociation takes place after electronic relaxation (internal conversion/intersystem crossing) from the initially excited state to a lower electronic state (electronic predissociation).

The proposed three-body photodissociation mechanism of *s*-triazine is similar to the one suggested for azomethane^{18,19} but differs from that of acetone. The latter has recently been reinvestigated by North et al.¹⁴ using photofragment translational spectroscopy and by Kim, Petersen, and Zewail¹⁷ by femto-second observation of the transient intermediate. Both groups established—contrary to some earlier claims⁴⁴—that the mechanism is stepwise and not concerted. The TOF spectrum of

the CH₃ photofragment showed two separate peaks due to CH₃ emerging from the primary and secondary dissociation step.

5. Conclusions

Following excitation at 308–193 nm *s*-triazine dissociates exclusively into three HCN fragments. At the six different excitation wavelengths used, only one single peak due to the HCN photofragment has been observed in the TOF spectrum, the analysis of which revealed the dissociation not to be a symmetric three-body process with a simultaneous breaking of the three bonds, but a sequential process with a short-lived intermediate H₂C₂N₂. The results of our photofragment distribution measurements and our conclusions thus contrast those of Ondrey and Bersohn⁸ who reported an anomalous behavior of $P(E_T)$, having a lower $\langle E_T \rangle$ at 193 nm than at 248 nm, and symmetric bond breaking. Furthermore, if we consider a rotational period or less of the intermediate, and in turn a correlation between the asymptotic velocity vectors of the three HCN photofragments, as a criterion of concertedness, the present dissociation process proceeds *in two steps but is concerted*. The features of the absorption spectrum in the excitation range 308–248 nm as well as those of the corresponding photofragment distributions $P(E_T)$ point to electronic predissociation. Hence, the initially excited state in *s*-triazine is in a first step electronically relaxed to a lower electronic state. The finally dissociative state is, according to symmetry correlation with three ground state HCN molecules, the electronic ground state S_0 (1A_1) of *s*-triazine.

Acknowledgment. Support of this work by the Schweizerischer Nationalfonds zur Förderung der wissenschaftlichen Forschung is gratefully acknowledged. J.A.H. acknowledges support from the Miller Institute for Basic Research in Science (Berkeley, CA) during the early stages of this research. We thank PD Dr. Peter Felder for valuable discussions, Dr. Philip R. Willmott for critically reading the manuscript, and Rolf Pfister for his assistance with the graphics.

References and Notes

- (1) Solomon, J.; Jonah, C.; Chandra, P.; Bersohn, R. *J. Chem. Phys.* **1971**, *55*, 1908.
- (2) Tamir, M.; Halavee, U.; Levine, R. D. *Chem. Phys. Lett.* **1974**, *25*, 38.
- (3) Korger, P. M.; Riley, S. J. *J. Chem. Phys.* **1977**, *67*, 4483.
- (4) Korger, P. M.; Riley, S. J. *J. Chem. Phys.* **1979**, *70*, 3863.
- (5) Kellman, M. E.; Pechukas, P.; Bersohn, R. *Chem. Phys. Lett.* **1981**, *83*, 304.
- (6) Baughcum, S. L.; Leone, S. R. *Chem. Phys. Lett.* **1982**, *89*, 183.
- (7) Dewar, M. J. S. *J. Am. Chem. Soc.* **1984**, *106*, 209.
- (8) Ondrey, G. S.; Bersohn, R. *J. Chem. Phys.* **1984**, *81*, 4517.
- (9) Zhao, X.; Miller, W. B.; Hints, E. J.; Lee, Y. T. *J. Chem. Phys.* **1989**, *90*, 5527.
- (10) Strauss, C. E. M.; Houston, P. L. *J. Phys. Chem.* **1990**, *94*, 8751.
- (11) Gruebele, M.; Roberts, G.; Zewail, A. H. *Philos. Trans. R. Soc. London* **1990**, *A332*, 223.
- (12) Khundkar, L. R.; Zewail, A. H. *J. Chem. Phys.* **1990**, *92*, 231.
- (13) Trentelman, K. A.; Kable, S. H.; Moss, D. B.; Houston, P. L. *J. Phys. Chem.* **1990**, *94*, 263.
- (14) North, S. W.; Blank, D. A.; Gezelter, J. D.; Longfellow, C. A.; Lee, Y. T. *J. Chem. Phys.* **1995**, *102*, 4447.
- (15) Wannenmacher, E. A. J.; Felder, P.; Huber, J. R. *J. Chem. Phys.* **1991**, *95*, 986.
- (16) Baum, G.; Felder, P.; Huber, J. R. *J. Chem. Phys.* **1993**, *98*, 1999.
- (17) Kim, S. K.; Pederson, S.; Zewail, A. H. *J. Chem. Phys.* **1995**, *103*, 477.
- (18) North, S. W.; Longfellow, C. A.; Lee, Y. T. *J. Chem. Phys.* **1993**, *99*, 4423.
- (19) Gejo, T.; Felder, P.; Huber, J. R. *Chem. Phys.* **1995**, *195*, 423.
- (20) Busch, G. E.; Mahoney, R. T.; Morse, R. I.; Wilson, K. R. *J. Chem. Phys.* **1969**, *51*, 449.
- (21) Wodtke, A. M.; Lee, Y. T. In *Molecular Photodissociation Dynamics*; Ashfold, M. N. R., Baggott, J. E., Eds.; Royal Society of Chemistry: London, 1987; p 31.

- (22) Pacansky, J. *J. Phys. Chem.* **1977**, *81*, 2240.
(23) Bolovinos, A.; Tsekeris, P.; Philis, J.; Pantos, E.; Andritsopoulos, G. *J. Mol. Spectrosc.* **1984**, *103*, 240.
(24) Goates, S. R.; Chu, J. O.; Flynn, G. W. *J. Chem. Phys.* **1984**, *81*, 4521.
(25) Osamura, Y.; Uonno, M.; Hashimoto, K. *J. Am. Chem. Soc.* **1987**, *109*, 1370.
(26) Benson, S. W. *Thermochemical Kinetics*, 2nd ed.; Wiley: New York, 1976.
(27) Byström, K. *J. Chem. Thermodyn.* **1982**, *14*, 865.
(28) Felder, P. *Chem. Phys.* **1990**, *143*, 141.
(29) Morley, G. P.; Felder, P.; Huber, J. R. *Chem. Phys. Lett.* **1994**, *219*, 195.
(30) Minton, T. K.; Felder, P.; Brudzynski, R. J.; Lee, Y. T. *J. Chem. Phys.* **1984**, *81*, 1759.
(31) Sparks, R. K.; Shobatake, K.; Carlson, L. R.; Lee, Y. T. *J. Chem. Phys.* **1981**, *75*, 3838.
(32) Zare, R. N. *Mol. Photochem.* **1972**, *4*, 1.
(33) Saigusa, H.; Lim, E. C. *J. Chem. Phys.* **1983**, *78*, 91.
(34) Hintsä, E. J.; Zhao, X.; Lee, Y. T. *J. Chem. Phys.* **1990**, *92*, 2280.
(35) Zhao, X.; Nathanson, G. M.; Lee, Y. T. *Acta Phys.-Chim. Sin.* **1992**, *8*, 70.
(36) Felder, P. Habilitationsschrift Thesis, University of Zürich, 1993.
(37) Miller, W. B.; Safron, S. A.; Herschbach, D. R. *J. Chem. Soc., Faraday Discuss.* **1967**, *44*, 108.
(38) Smith, D. J.; Grice, R. *Mol. Phys.* **1991**, *73*, 1371.
(39) Zhao, X.; Hintsä, E. J. *J. Chem. Phys.* **1988**, *88*, 801.
(40) Krajnovich, D.; Huisken, F.; Zhang, Z.; Shen, Y. R.; Lee, Y. T. *J. Chem. Phys.* **1982**, *77*, 5977.
(41) Butler, L. J.; Buss, R. J.; Brudzynski, R. J.; Lee, Y. T. *J. Phys. Chem.* **1983**, *87*, 5106.
(42) Wodtke, A. M.; Hintsä, E. J.; Lee, Y. T. *J. Phys. Chem.* **1986**, *90*, 3549.
(43) Innes, K. K.; Ross, I. G.; Moomaw, W. R. *J. Mol. Spectrosc.* **1988**, *132*, 492.
(44) For a discussion see ref 17.

JP9609592